Measurements of the trace level of radioactivity in materials for use in the SNO+ and nEXO experiments at SNO Lab

By

Mona Alsubaie

Thesis submitted to the
Faculty of Graduate and Postdoctoral Studies
In partial fulfillment of the requirements
For the M.Sc. degree in
Physics

Ottawa-Carleton Institute of Physics
Faculty of Science
University of Ottawa

Abstract

Radioactive isotopes are present at some level in all materials in our environment. Detection of these isotopes by conventional means can be difficult if they decay very slowly (have a long half-life). Accelerator Mass Spectrometry (AMS) systems are actually designed to measure extremely low levels or such isotopes. Such measurements are often useful for dating geological processes and archaeological artifacts or tracing chemical pathways through complex systems.

In the search for very rare processes such as neutrinoless double beta decay, the presence of very low levels of radioactive material can interfere with the measurement process. Therefore, materials used to build the experimental equipment have to contain as few radioactive isotopes as possible.

Neutrinoless double beta decay (NDBD) is of interest for understanding whether the neutrinos are Dirac or Majorana particles. SNO+ and nEXO are among the experiments at SNO Lab, located in Sudbury, Canada for the detection of neutrinos and other extremely weak physical processes.

The SNO+ detector is a large 12m diameter spherical scintillation counter which will be able to study low energy solar, geo- and reactor neutrinos, as well as being able to conduct supernova searches. This detector was built with materials with very low radioactivity such as the organic liquid, Linear Alkyl Benzene (LAB), the scintillation fluid in which the radioactivity was measured in earlier scintillation detectors. For NSBD measurements, the SNO+ experiment will add tellurium-130 to the LAB; In order to fully mix the ^{130}Te into the LAB, the liquid 1, 2 Butanediol has been selected as a chelating agent to which the atoms of ^{130}Te can be added. This project describes the measurement of the ^{14}C content of the 1, 2 Butanediol which confirmed its suitability for use in the NDBD experiment.

nEXO is the next in a series of experiments dedicated to the search for NDBD in Xenon-136. The nEXO detector is a time projection chamber (TPC) filled with 5000 kg of liquid Xe. One major source of reduction in sensitivity of this detector is the radioactive decay of trace amounts of uranium and thorium isotopes naturally present the construction materials. In order to assess the quantity of these isotopes in the copper used to make the electrodes in the TPC, samples of the copper to be used in the chamber were analyzed using AMS. In this measurement, a better source of copper was found.

Acknowledgments

Above all, I thank Allah Almighty who enabled me to finish this work despite many challenges. I would like to express my deepest gratitude to my supervisor **Dr. Liam Kieser** for the guidance, encouragement and advice he continuously provided me with. I have been extremely lucky to have a supervisor who cared so much about my work, and who responded to my questions and queries so promptly. I owe a lot of gratitude to the University of Ottawa AMS members, **Sarah Murseli**, for her help in preparing the samples and **Dr. Xiaoei Zhao**, who contributed and extended his valuable assistance in the preparation and completion of this research work. A special thanks to my husband, **Ayidh**, for his endless support and great patience at all times. This thesis would not have been possible without his encouragement and continuous help. My accomplishments are due, in large part, to the massive contribution from my family. This work would not have been possible without my parents, **Sarah & Mohammed**, my sister **Eidah** , my uncle **Abdullah** and my aunt **Haya** who have always supported me emotionally and financially. I also dedicate this thesis to my lovely kids; **Abdullah & Mohammed,** being with you always brought me the greatest joy and happiness in life. Praise is to Allah for giving me such a great family. I am very thankful to my country Saudi Arabia for awarding me with **King Abdullah bin Abdul-Aziz** scholarship administered by Saudi cultural bureau in Canada to pursue my graduate studies at the University of Ottawa. Last but not the least; I would like to thank my friends, Soha, Zakiah, Nadrah and Naema for their endless love and support that have made the hard times so much easier.

Content

List of Tables

List of Figures

List of Abbreviations

AMS	Accelerator mass spectrometry
AMU	Atomic Mass Unit (Dalton) 1.661×10^{-27} kg
SNO	Sudbury Neutrino Observatory
EXO	the Enriched Xenon Observatory
TIMS	Thermal Ionization mass spectrometry
SNEWS	Supernova Early warning system
LS	Liquid Scintillator
WIPP	Waste Isolation Pilot plant
LAB	Linear Alkyl-benzene
NDBD	Neutrinoless double beta-decay
TPC	Time Projection Chamber

Chapter 1

1.1 Radioactive Decay:

Nuclear decay (also called radioactive decay) is the process in which an unstable atomic nucleus proceeds from a higher energy state to a lower energy state. The energy released is transferred to certain particles that are emitted [1]. The type of particle emitted depends on the type of nuclear decay, and these particles constitute what is referred to as nuclear radiation. There are three major types of nuclear decay: alpha, beta, and gamma. Alpha decay involves ejection of a helium nucleus (two protons, and two neutrons) from an unstable core, resulting in a decrease in the atom's atomic number by two. Beta decay involves the ejection of an electron and an antineutrino from an unstable nucleus, resulting in the conversion of one neutron into one proton. Alternatively, if a positron and a neutrino are emitted, a proton in the nucleus is changed into a neutron. Gamma decay involves the electromagnetic emission of a high energy photon from an unstable nucleus [2].

The law of radioactive decay

$$A = dN/dt = \lambda N \qquad (1)$$

$$\lambda = \ln(2) / t_{1/2} \qquad (2)$$

$$N = N_0 e^{-\lambda t} \qquad (3)$$

Where A = activity (decays per unit time), dN = number of atoms, $t_{1/2}$ is the half life and λ is the decay constant.

1.2 The Neutrinos

Neutrinos are subatomic particles named as such based on their neutral charge and small mass, in fact having a significantly lower mass than all other elementary particles. Because the

neutrino is known to have a ½ integer spin and does not undergo strong interactions (that is, not affected by the strong nuclear fundamental force), it is classed as a lepton. The nature of these particles that are unperturbed by strong interactions and have non-zero but miniscule masses causes them to be nearly undetectable, as they will generally pass through matter. Neutrinos come in three flavors: electron, muon, and tau after the particle that they are associated with in the decay process. Al though minor variations between these types of neutrinos exist, a single neutrino will exist in a quantum superposition of the three and during motion a neutrino will oscillate between the three flavors [3].

Neutrinos are produced during the standard beta decay of atomic nuclei (or hadrons), as well as through nuclear reactions as seen in the core of stars and supernovae. They can further be produced as particle accelerators smash atoms, or through interaction of atoms with cosmic rays. To date, the theoretical (mathematically demonstrated) difference between of the masses of the three flavors of neutrinos has not been shown experimentally, but further analysis suggests their mass to be about 1/1000,000th that of an electron[1]. Wolfgang Pauli first hypothesized the existence of neutrinos in the 1930s ^{as} a means to describe the conservation of spin, momentum, and energy that occurs during beta decay [4]. This hypothesis was coupled with the fact that electrons or beta particles were the product of beta decay. It was not until 1956 that Cowan et al [4] detected the neutrino using a method of Beta-capture proposed by Wang Ganchang. This was added to by determining the handedness (chirality) of neutrinos being measured by C. S. Wu, who described neutrinos as having left-handed chirality. The 2002 Nobel Prize in physics was jointly awarded to physicists who described the nature of solar neutrinos and the direct observation of supernovae neutrinos [5]. The discovery of neutrino oscillation marked a

significant turning point in neutrino physics- where neutrino with specific lepton flavor was found to possess oscillating characteristics [3].

1.3 Double Beta Decay

Normal double beta decay involves ejection of two electrons and two antineutrino particles at the same time from an unstable nucleus. This occurs when single beta decay is not allowed by the ground stat energy of the neighboring nucleus. This process leads to the conversion of two protons into two neutrons in the atomic nucleus see (Figure.1) [8]. The process of double beta decay was first envisioned by Maria Goeppert-Mayer in 1935 [11]. Despite being proposed in the 1930s , double beta decay was not actually observed until 1987 in the Michael Moe lab at UC Irvine [7]. This process is exceedingly rare (rarer than all other forms of nuclear decay), and so far has been observed in only twelve isotopes including ^{48}Ca, ^{76}Ge, ^{78}Kr, ^{82}Se, ^{96}Zr, ^{100}Mo, ^{116}Cd, ^{128}Te, ^{130}Te, ^{136}Xe, ^{150}Nd, and ^{238}U [17] See table 1.

In order for double beta decay to be possible, the resulting nucleus must possess a higher binding energy than the parent nucleus. In 1939, Wendell Furry proposed the concept of neutrinoless double beta decay based on the work of Ettore Majorana: that double beta decay could proceed without emission of antineutrinos if they were Majorana particles. The theory of neutrino-less double beta decay is based on the classification of fermion particles (particles that spin at one half integer and comprise quarks, leptons, and composite particles) into two categories – the first category is Dirac fermions which have a specific charge and for these particles, each has a corresponding antiparticle with the opposite charge (ex. the negatively charged electron, and the positively charged positron). The second category is a theoretical category called Majorana fermions, first envisioned by Ettore Majorana [15]. These particles do not have a corresponding antiparticle and are their own antiparticle (their wave equation is

identical to their antiparticle) and because it exists as both particle and antiparticle with opposing charges, the Majorana particle would have a neutral charge The process of neutrinoless double beta decay is thought to involve two beta decay events occurring simultaneously followed by a subsequent annihilation of the produced antineutrinos (since they are their own antiparticle in the Majorana theory, they would have the ability to annihilate each other) [10] see (Figure.2). Currently it is debated whether neutrinos are Dirac or Majorana, and if they are the latter then double beta decay is possible.

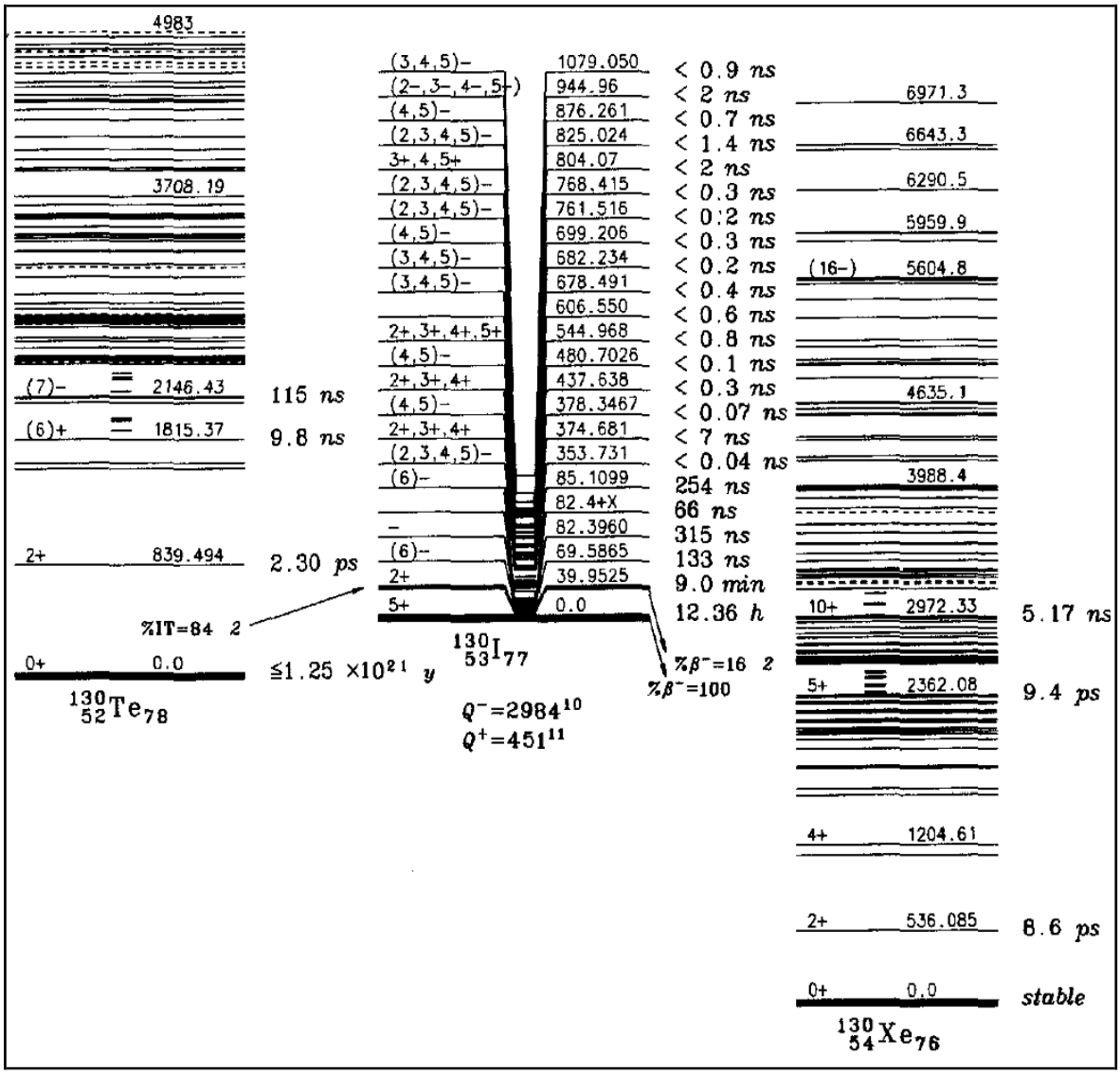

Figure 1: Part of the energy level scheme for mass = 130 AMU isotopes that shows the energy conditions by which the single beta decay transition from ^{130}Te to ^{130}I is forbidden and that the double beta decay from ^{130}Te to ^{130}Xe is allowed [12].

Table 1: Neutrinoless double beta decay candidates with their corresponding Q- value and natural abundance.

Isotope	G 0ν (10^{-14} y^{-1})	$Q_{\beta\beta}$ (KeV)	Nat. ab (%)
^{48}Ca	6.35	4273.7	0.187
^{76}Ge	0.623	2039.1	7.8
^{82}Se	2.70	2995.5	9.2
^{96}Zr	5.63	3347.7	2.8
^{100}Mo	4.36	3035.0	9.6
^{110}Pd	1.40	2004.0	11.8
^{116}Cd	4.62	2809.1	7.6
^{124}Sn	2.55	2287.7	5.6
^{130}Te	4.09	2530.3	34.5
^{136}Xe	4.31	2461.9	8.9
^{150}Nd	19.2	3367.3	5.6

In 2014, researches at Princeton University found evidence that supported the existence of Majorana bound states in experiments involving scanning tunneling microscopes, and these states were implicated in superconducting lead researchers at the Oak Ridge National Laboratory demonstrated that Majorana fermions existed as quasi particles in solid state material [16][6]. If these experiments are demonstrating the existence of neutrino-less double beta decay, this would support the idea of Majorana fermions existing, and could have interesting implications, such as a possible explanation for what dark matter is comprised of in the field of astronomy [14].

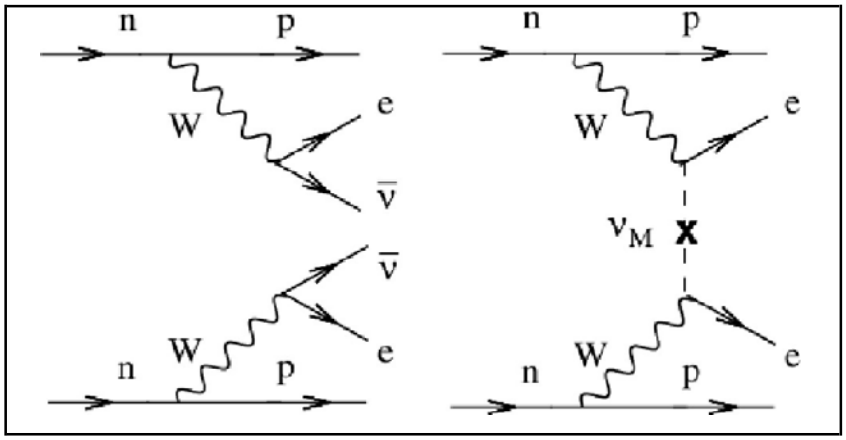

Figure 2: Feynman diagrams for ordinary (left) and neutrinoless (right) double beta decay. NDBD violates total lepton number by two units and is forbidden according to the Standard model. [13]

1.4 The SNO+ Experiment

In order to understand the neutrinos, it is imperative to detect neutrinos, Due to the weak interactions of neutrinos with matter, detectors must contain large quantities of matte.. They are usually built underground to reduce interference from cosmic radiation [20], [21]. The Sudbury Neutrino Observatory is one example, located in Creighton Mine, operated by the mining company Valé in Sudbury, Ontario. The original detector operated by detecting Cherenkov radiation. This radiation occurs when neutrinos interacts with matter to create an electron in the heavy water (D2O), used as the detection medium. Photomultiplier tubes were used to detect the Cherenkov light, indirectly detecting the neutrinos. The detector consisted of an acrylic sphere filled with 1000 tones of ultra-pure D2O, surrounded by 7000 tones of H2O and 9500 photomultiplier tubes [19]. SNO+ uses the original detector chamber but replaces the D2O with Linear Alkyl Benzene (LAB) which is a more sensitive detector of neutrino. One of the experiments to be carried out on this detector is a search for neutrinoless double beta decay (NDBD). Its studies also include the detection of supernovae neutrino, solar neutrinos and

antineutrinos, as well as the measurement of the natural radioactivity of the earth. The SNO+ detectors will be a new kiloton scale liquid scintillator detector that will be study neutrinos with one goal being the observing neutrinoless double beta decay [22][23].

Three main data talking phases are planned: 1) the detector filled with ultrapure water, 2) the detector with unloaded liquid scintillator and 3) with 2.34 tones of tellurium loaded into the detector. Two neutrinos double beta decay is a very rare process that is permitted for 35 known natural isotopes, 11 of which are listed in table 1. It was experimentally observing 12 of them one of them 130 Te. The background introduced by this material will be studied in Chapter 3.

1.5 The Enriched Xenon Observatory Experiment:

The Enriched Xenon Observatory (or EXO) is a large experiment dedicated to discovering neutrinoless double beta decay in the Xenon-136. The equipment for the initial experiment is located in Carlsbad, New Mexico, in an underground laboratory, the Waste Isolation Pilot Plant (WIPP), run by the US Department of energy. Many international institutions are involved in this research, with a group dedicated to this research at Carleton University in Canada along with many universities across the US and Canada. There are two stages in the enriched xenon experiment [24]. The first is the EXO-200, which is a large prototype experiment containing 200 kg of Liquid Xenon which has already made it possible to measure the two neutrino-mode of double beta decay of the Xenon-136 isotope of Xenon. Through the data generated with EXO-200, a more stringent limit of the rate of neutrinoless double beta decay has been ascertained. While this is an achievement in itself, the EXO-200 remains in operation at WIPP with the US Department of Energy and continues to collect data

that can potentially lead to the discovery of the double beta decay Furthermore, EXO-200 has the potential to provide a more accurate measurement of the two neutrino double beta transition [25].

The second stage is nEXO (or next EXO). This will use an improved Xenon detector which contains 5000 kg of liquid Xenon for observing the NDBD process using the time projection chamber measurement of the beta particles and a way to tag or mark the barium-136 daughter ion which is produced by the decay. By effectively confirming the presence of this ion, scientists can essentially eliminate noise, or the background interferences, from the decay of unrelated isotopes [26]. Currently, this part of the EXO experiment involves the extraction and tagging (marking) of the double beta decay progeny While there has already been much learned from EXO-200, the nEXO experiments is still in the design stage and will continue and will begin gathering more data with more discoveries well into the future [25]. In chapter 4 provides details about the Next Enriched Xenon detector (nEXO).

1.6 Overview of the thesis

This chapter introduces the goals of SNO+ and nEXO. The aim of this research is to measure the trace level of contamination for isotopes. These isotopes will be used in the neutrinoless double beta decay experiment that is highlighted into two experiments: SNO+ at the Sudbury Neutrino Observatory and The Next Enriched Xenon Observatory (nEXO). However, one of the most significant challenges is the presence of very low levels of radioactive material that can interfere with the measurement process. The analytical procedure by AMS is effective in the separation of uncommon isotopes from abundant adjacent isotopes. In this work, we determine the trace level of radioactivity in the liquid 1,2-Butanediol for SNO^{+} and copper for nEXO using Accelerator Mass Spectrometry (AMS). For the measurement of the neutrinoless process (NDBD), in order to distribute the ^{130}Te throughout the LAB, the nEXO group plans to use 1,2, Butanediol as a chelating agent. The common theme in these measurements is the

necessity to reduce the “memory effect” in the AMS ion source so that other measurements do not contribute contaminants and cause our measurement to show a higher level of the radionuclide than actually is in the sample.

Regarding the ^{14}C measurements presented in this thesis which were taken under the supervision of Sarah Murseli, I prepared the LAB and Butanediol samples and was present during the preparation of the AMS system and collection of the data. The copper samples were prepared for us by the nEXO group but I was present during the preparation of the AMS system and data collection.

Chapter 2

2.1 Accelerator mass spectrometry

Accelerator mass spectrometry (AMS) is a method of mass spectrometry that measures isotopes ratios below 10^{-12} [28]. It uses an accelerator along with ion sources, electric analyzer, magnets, and a detector to measure a single rare atom in the presence of up to 1×10^{-15} abundant or stable atoms. In this technique, as opposed to the basic mass spectrometer, the molecular interferences are removed by their destruction during the charge-changing collisions at a few million electron-volts (eV) energy inside the accelerator. The accelerator produce even higher energy by enables AMS to measure a range of elements and isotopes as wide as from ^{3}H to ^{244}Pu [29]. The negative ions created in the ion source occasionally result in the suppression of unwanted isobars; an example is ^{14}N in the case of ^{14}C analysis, which is suppressed as a result of its inability to form negative ions (anions). In addition to injection atomic anions, for elements that do not easily form anions, AMS can inject them as molecular anions. A typical example is the used of fluorine to form molecular anion of the actinides, e.g. PuF_4^-. An AMS system contains the same parts as a basic mass spectrometer: an ion source, several magnets and detectors, plus an accelerator (see Fig. 2)

AMS selects ions based on their energy/charge (E/q) and mass x energy/charge squared ($m\ E/q^2$) that can be change in a controlled manner as the ions pass through the spectrometer, and this helps to separate the isotopes [28]. A third type of analyzer, not used on the Ottawa system is the velocity analyzer, which measures the ratio of E/q and M/q. All these three detectors are used in suppressing unwanted ions that often arise from slit scattering or molecular fragmentation [28].

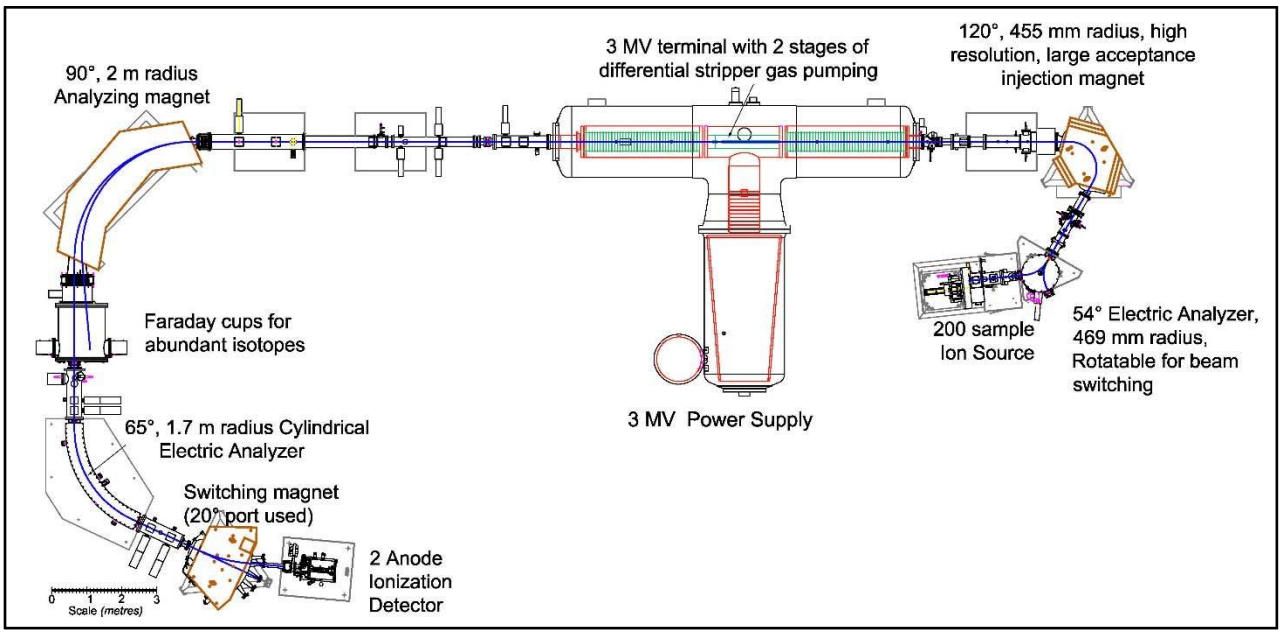

Figure 3: Schematic representation of AMS indicating its components [29].

In general, the force on an ion is given by

$$\mathbf{F} = q(\mathbf{E} + \mathbf{v} \times \mathbf{B}) \qquad (2.1)$$

Where $\mathbf{E}$ and $\mathbf{B}$ are the electric and magnetic fields, q is ion charge and $\mathbf{v}$ is velocity of the ion

(vectors are denoted by bold face type)

For a magnet $\mathbf{F} = q\,\mathbf{v} \times \mathbf{B}$ (2.2)

by combining $\mathbf{F} = m\mathbf{v}^2/R$ and $E = m\mathbf{v}^2/2$, where m is the mass of the ion, R is the radius of the trajectory and E is the kinetic energy of the ion, the value of the field $\boldsymbol{B}$ is given by

$$\mathbf{B} = \sqrt{2mE}\,/\,qR \qquad (2.3)$$

Thus, to tune a magnet for a different mass, its field $\mathbf{B}$ has to be adjusted in proportion to the square root of the mass m; similarly, for a change in energy E, the field $\mathbf{B}$ has to be adjusted in proportion to the square root of the energy E.

Similarly, for an electric analyzer: $\mathbf{F} = q\,\mathbf{E}$, and so $\mathbf{E} = 2E / qR$ (2.4)

so, for tuning the electric analyzer, as the analyzer electtodes (plates) are a fixed distance apar, the field $\mathbf{E}$ can be adjusted by changinging the voltage difference across the plates in proportion to the change in ion beam energy.

While the rejection ratio of each of these analyzers is around a factor of about 10^{+5}, generally, a combination of the analyzers or a series arrangement of one of each of the analyzers can yield a rejection ratio of 10^{+15} which is good enough for nearly all AMS analysis [28]. The accelerator used in the AMS system is often the tandem accelerator because it uses two acceleration sections in a line, Following the acceleration of the negative ions to the central electrode of the tandem, these negative ions pass through an argon filled canal to strip off two or more of the electrons, thus making the ions positively charged and breaking up molecular anions. The ions is then accelerated again through the same high voltage, following a second set of analyzers selects the ions of interest and the number of atoms is counted in the gas ionization detector. The following sections outline the method used by AMS to counts the isotopes directly, using of radiocarbon as an example.

2.2 SO-110/200 Ion Source:

The SO-110/200 ion source is used to analyses all isotopes on the A.E Lalonde Laboratory AMS system. This source was developed to provide analyses for large numbers of ^{14}C samples in both graphite and CO_2 gas [30], [34]. Recently, there has been a rising demand for rapid sample measurement, which requires sufficient capacity for the preparation of the samples, along with fast measurements and minimal system downtime. However, for higher measurement efficiency, the

AMS system requires a high ion current output, without compromising the reproducibility of the measurement or a disproportional increase of the maintenance. This ion source is capable of being run at outputs of up to 200 μA $12C^{-}$. "These early measurements indicate for a 200 μA ^{12}C source output, equivalent to a □1 kHz ^{14}C count rate for Ox II samples, a $^{13}C/^{12}C$ precision of 1% and a $^{14}C/^{12}C$ precision of 0.3% can be obtained" [32]. For the ion source used on the Lalonde AMS, an output of the cesium sputter ion source has been upgraded compared to the original SO-110 model [30]. The ion source must provide high, stable currents of the analyze ions.

A schematic of this source is shown in Figure 4. The sample, e.g. carbon in form of graphite, is compressed into a small pellet in a metal holder. This assembly is known as a target. Atoms in the target are converted into negative ions in the following way. Cesium ions are formed by spraying Cs vapour onto the hot (1200°C) ionizer surface. The cesium ions move quickly because of the voltage between the ionizer and the target (7000 volts). This voltage also focusses the ions to hit the target sample very tightly, about 1 ml in diameter. The heavy Cs ions knock the carbon atoms out of the target. This process is called sputtering. Figure 2 shows the pathways taken by the Cs and sample ions. After collision with the target, the cesium atoms remain on the target surface and form a thin Cs layer. When the carbon atoms pass through this layer, some of them pick up an extra electron and become anions, After being ionized, they will be moved by the electrical fields out of the source and became a negative carbon ion beam.

After the ion source, the ions are separated by mass as they exit the magnet as the beam of carbon ions. The ions produced are then directed to the accelerator where there is collision with gas molecules hence breaking them. For instance, $^{12}CH_2$ can be disintegrated into $^{12}C^{3+}$ ions

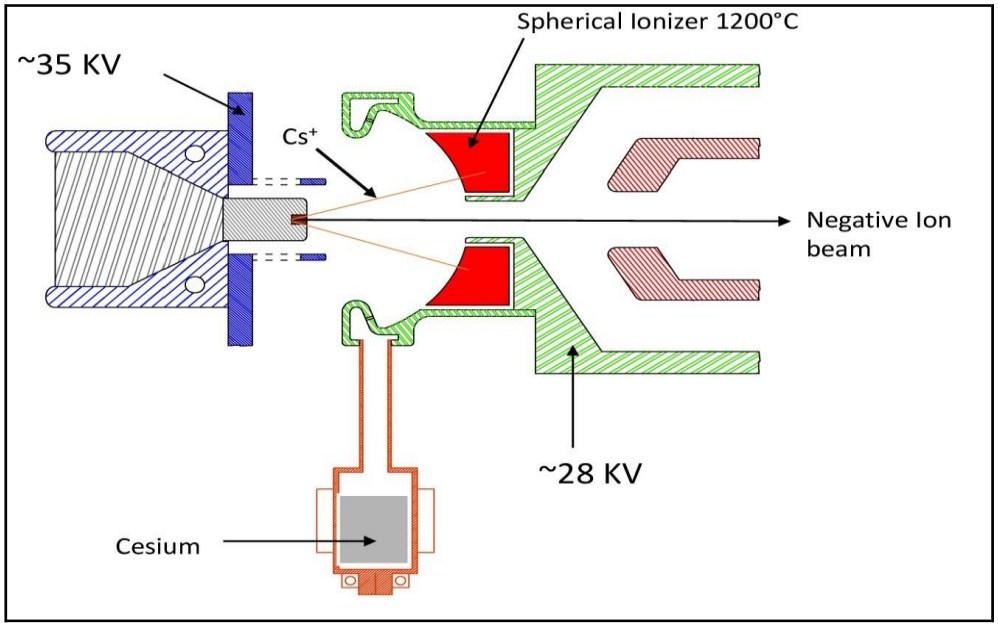

Figure 4: AMS ion source schematic [18].

through the removal of the existing 4 electrons. These ions are further accelerated and then a second magnet picks ions that achieve the required momentum of ^{14}C ions. The final the process entails counting of the ^{14}C ions by the gas ionization detector where the velocity and energy of the ions are reduced by collisions with isobutene gas. Effectively, this ensures that the number of ^{14}C ions in the given sample can be tallied. That is, this technique effectively subdues molecular isobars. Moreover, this method can be used to successfully detach atomic isobars.

Ion source Memory

Much of the sample material comes away from the target unionized, as sputtered neutral atoms and these can become attached to nearby surfaces surrounding the target (e.g. field shaping electrode, ionizer shroud and ionizer itself). These deposited atoms can be released during the analysis of later samples and, if re-ionized and included in the primary sputter ion beam, they are then implanted into the later samples. This recycling phenomenon results in the contamination of

the sample being analyzed by samples analyzed earlier, also know as the ion source “memory effect”. Although it is small for normal analyses, for samples with very low isotope ratios it must be assessed.

2.3 Accelerator and Electron Stripping Canal

The AMS has a specialized section known as the accelerator, composed of a medium current (750 μA), 3.0 Megavolt Tandetron, fitted with 21 Gigaohm resistor divider chains attached on the low and high energy accelerator tube electrodes [29], to ensure stable acceleration conditions. The electron stripper canal in the high voltage terminal of this accelerator consists of an open tube 10 mm in diameter and 700 mm long which is pumped at each end into a larger volume (150 mm diameter) by a turbo pump. The exhaust of the turbo pump is returned to the center of the canal along with a small quantity of make-up gas. The gas pressure in the canal is measured by a vacuum gauge and controlled by automatically adjusting the flow of make [up gas]. This pressure can be modified according to the kind of analysis needed. The stripping canal in this AMS contains a secondary phase of differential pumping at the exit of the stripper canal. Essentially, this ensures that the pressure in the high energy tube is further minimized while sustaining the pressure in the low energy tube closer to that attained in a lone turbo pump system [32, 33].

2.4 High Energy Analysis and Detectors

The detectors system in AMS entails a string of processes that are necessary for the analysis of a given sample. The positive ions that exit the stripper canal (in charge state 3+ for

carbon ions) are further accelerated where a second magnet picks ions that achieve the required momentum of ^{14}C ions. Therefore, given a certain carbon ion a preset charge state, and a fixed magnetic field, the separation process of the carbon molecule can be ascertained as explained above using the formulae provided. The final process entails filtering of the ^{14}C ions by the magnets and electric analyzer where the momentum and energy are ascertained. The detection process for the much more abundant ^{12}C and ^{13}C ions uses two Faraday cups, located after the first magnet, to measure their electrical current. The ^{14}C ions proceed on through an electric analyzer and a second magnet to the Gas Ionization Detector which counts the individual ^{14}C atoms. This provides information which can be utilized to obtain the amount of ^{14}C and its ratio in comparison to ^{12}C and ^{13}C.

2.5 Summary

This chapter gives a detailed description the experimental techniques used for the present work. The first section describes how the accelerator mass spectrometer provides highly sensitive isotope ratio measurements for a wide variety of applications, by having three components: the ion source and low energy analysis system, the accelerator and the high energy analysis and detection system. The second section provides more details of the operation of the Cs sputter source and the production of negative ions. The next section discusses the accelerator and its electron stripper canal and the final section outlines how the high energy positive ions are accelerated to a sufficient velocity for separation and analysis in the detection system.

Chapter 3
Measurements for SNO+ Materials:

3.1 linear Alkyl Benzene (LAB)

As introduced in section 1.4, the organic liquid scintillator that SNO+ has decided to use is Linear Alkyl Benzene (LAB) which will replace the heavy water used in the original detector. This material was chosen due to its high light yield, fast decay, chemical compatibility with acrylic vessel (any degradation of the acrylic vessel or other components through contact with the scintillator is unacceptable), as well as its safety requirements. To use the LAB scintillator, with a density of 0.86, the acrylic vessel (AV) had to be re-engineered to take up large buoyant force, as opposed to the downward force in effect when heavy water was used in the detector. Also, the radio purity of the system is strictly controlled, with a newly built calibration deployment system that helps to avoid Radon contamination. However, unlike SNO, a high frequency calibration with internally deployed sources is not feasible, due to the risks of contamination. Nevertheless, the SNO+ detector, which is situated under the ground can reduce this interference.

Furthermore, LAB is a basic component in many household detergents which means that it is available at low price without excessive shipping costs. There is a plant in Quebec that produces very good LAB. Among the characteristics of the LAB are high light yield to convert energy with materials, it long time stability and high flash point. The acrylic compatibility good optical characteristics of linear alkyl benzene make it a good choice for the SNO+ liquid scintillator.

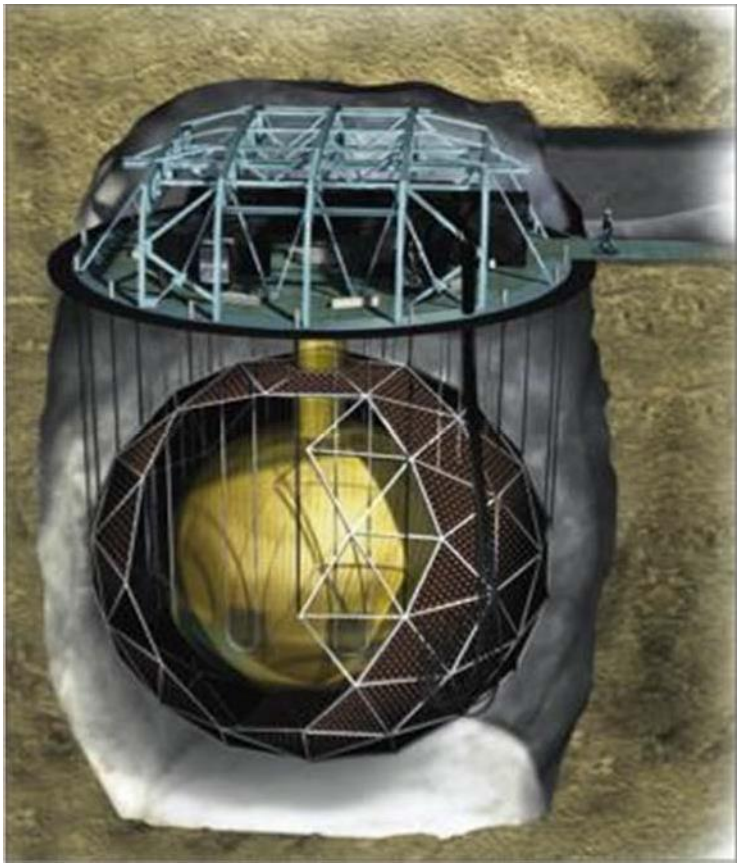

Figure 5: Schematic diagrams of the SNO detector [37].

3.2 Tellurium-loaded scintillator and 1, 2butanediol

The SNO+ project plans to incorporate Tellurium130 in the scintillation liquid to detect the neutrinoless double-beta decay, in which the two neutrinos produced annihilate each other. Detection of this process would prove that neutrinos act as their own anti-particles and would shed light on the Majorana nature of neutrinos. Using Tellurium130 over several years, while gathering data, will allow the measurement of the Majorana Neutrino mass below the 100 mev threshold. Tellurium in the form of telluric acid Te (OH) 6 is reacted with 1, 2 butanediol to form adiol complex (Te-diol) that is then dissolved into the LS (TeLS). The production reaction is shown in Figure (6). ^{130}Te exists at an abundance of 34.1% in natural Te and decays to ^{130}Xe

via double beta decay. The resulting complex is soluble in LAB and will allow for the target loading of 0.5% Te by mass in the detector [3.8].

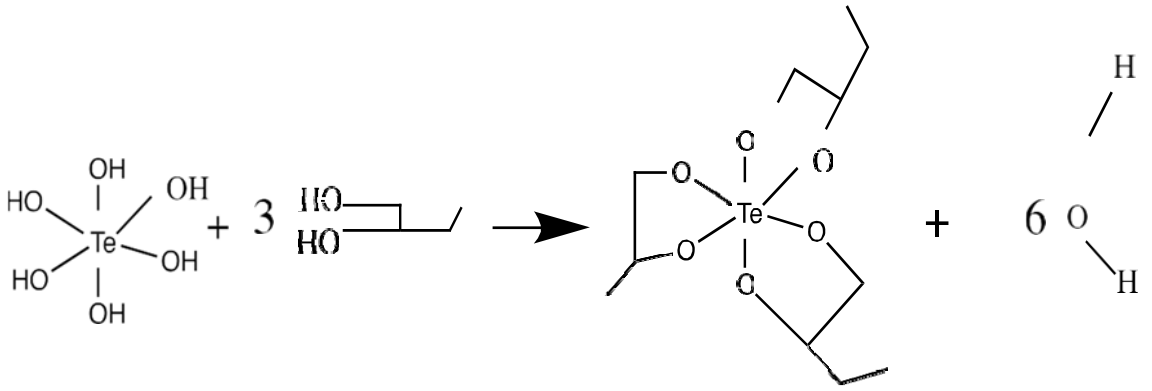

Figure 6: Reaction of telluric acid and 1,2-Butanediol to produce the tellurium complex [39].In this diagram, the C and hydrogen H atoms in the 1,2 Butanediol are not shown.

3.3 First measurement [twenty low background samples]

3.3.1 Sample Preparation

Before the samples can be analyzed in the AMS-system, the carbon in them has to be extracted and converted into the form of graphite. This is a three stage process involving first combustion, then clean-up of the resulting CO_2 gas and then graphitization. There were two materials from which samples were prepared, Linear Alky Benzene and 1, 2 Butandiol of which 5 aliquots of each were prepared. For each sample, two combustion methods were used. For the preparation of normal samples for ^{14}C analysis, samples can either be sealed with an oxidizer in an evacuated quartz tube and heated for about 1 hour at ~600°C or be combusted in an Elemental Analyzer, trapping the CO_2 from the exhaust strea As these samples were expected to have very low levels

of ^{14}C and as they were liquids, both methods were used to determine which would incorporate the least ^{14}C contamination:

1. In the first method, an aliquot of each sample was weighed into a quartz tube, with an excess of copper oxide (CuO). That is, sufficient CuO was used to give more than enough oxygen so that when the samples were heated, they were completely oxidized to carbon dioxide instead of carbon monoxide. After solidifying the sample by immersing the tube in liquid nitrogen, the tubes were evacuated and sealed with a torch. The sealed tubes were placed in an oven at 600° C for 1 hour to release the oxygen from the CuO and to combust the sample. After the samples had cooled, the quartz tubes were broken in a vacuum chamber and the gas was passed through a system to remove the water vapor by using a trap cooled by dry ice and alcohol to -40°C. The CO_2 sample was then deposited as a white powder in a trap cooled with liquid nitrogen (-196°C) and any remaining non-condensable gases (e.g. argon) were pumped away. The trap was then isolated from the vacuum pump (the valves on either side of this trap were closed) and the CO_2 in it was allowed to sublimate. When it reached room temperature (20°C) the pressure of the CO_2 was measured to determine the yield of the reaction. The CO_2 was then transferred to a pre-baked Pyrex break seal for storage and transfer to the graphitization line.

2. In the second method, samples were combusted using a Thermo Flash 1112 elemental analyzer (EA), operated in CN mode and interfaced with an extraction line to remove water vapor and non-condensable gases, similar to that used in the first method. For introduction into the EA, the liquid sample was weighed into a silver capsule which was sealed under a flow of helium gas to remove any atmospheric CO_2. Then the purified CO_2 was sealed in a pre-baked 6-mm Pyrex break seal.

After the CO_2 clean-up, the sample has to be prepared by graphitization in which samples are converted into solid graphite. Samples of pure CO_2 in 6-mm break seals are converted to elemental carbon in the presence of iron and hydrogen using semi-automated graphitization lines which consist of 10 reaction modules and their support equipment (vacuum pumps, chiller and process gas feeds. that were designed and built in-house. In brief, 10 break seals are scored, loaded into cracker tubes, and a small amount (4 mg) of iron powder that functions as a catalyst is placed in the quartz reaction tubes. The cracker tubes are left to pump overnight along with the reaction tubes. To remove any possible carbon in the iron powder, it is first conditioned by

- Introducing 700 mBar of oxygen into the reaction cell
- Heating it to 500°C for about 1 hour
- Cooling the reaction cell and pumping away any resulting CO_2 and excess oxygen
- Introducing 700 mBar of hydrogen
- Heating the reaction cell to 500°C for an hour to reduce the iron oxide back to iron powder
- pumping away the remaining H_2 and water vapour, then freezing the remaining water vapour into the cold trap."

After conditioning the iron, the CO_2 is released into the reactor by gently creating a bend at the Rolex cracker joint to snap the break seal, followed by transfer to the reaction volume by freezing into the water trap using liquid nitrogen. Residual non condensable gases are pumped away; the CO_2 is heated back to room temperature to check the pressure, and then refrozen to add hydrogen into the reaction volume at 2.5× pCO_2. Ovens are connected and the quartz tubes are heated to a reactor inside temperature of ~550°C. The pressure, oven temperature, and cooling cup (water trap) temperatures for each sample are monitored, graphed, and recorded throughout

the reaction. The cooling assembly was designed to provide equal, uniform cooling for each reaction module to optimize water extraction during graphitization. All operations on the line are controlled with a touch screen monitor using a Labview program [40]. Together with H_2 gas, in the presence of the iron powder, the CO_2 is converted into solid graphite and water.

$$CO_2 + 2H_2 \rightarrow C + 2H_2O$$

We have to remove the water by freezing it in a trap immersed in a cooling cup. The screen graphics monitoring the entire process are shown in Fig 7 for the Butanediol samples and Fig 8 for the LAB samples.

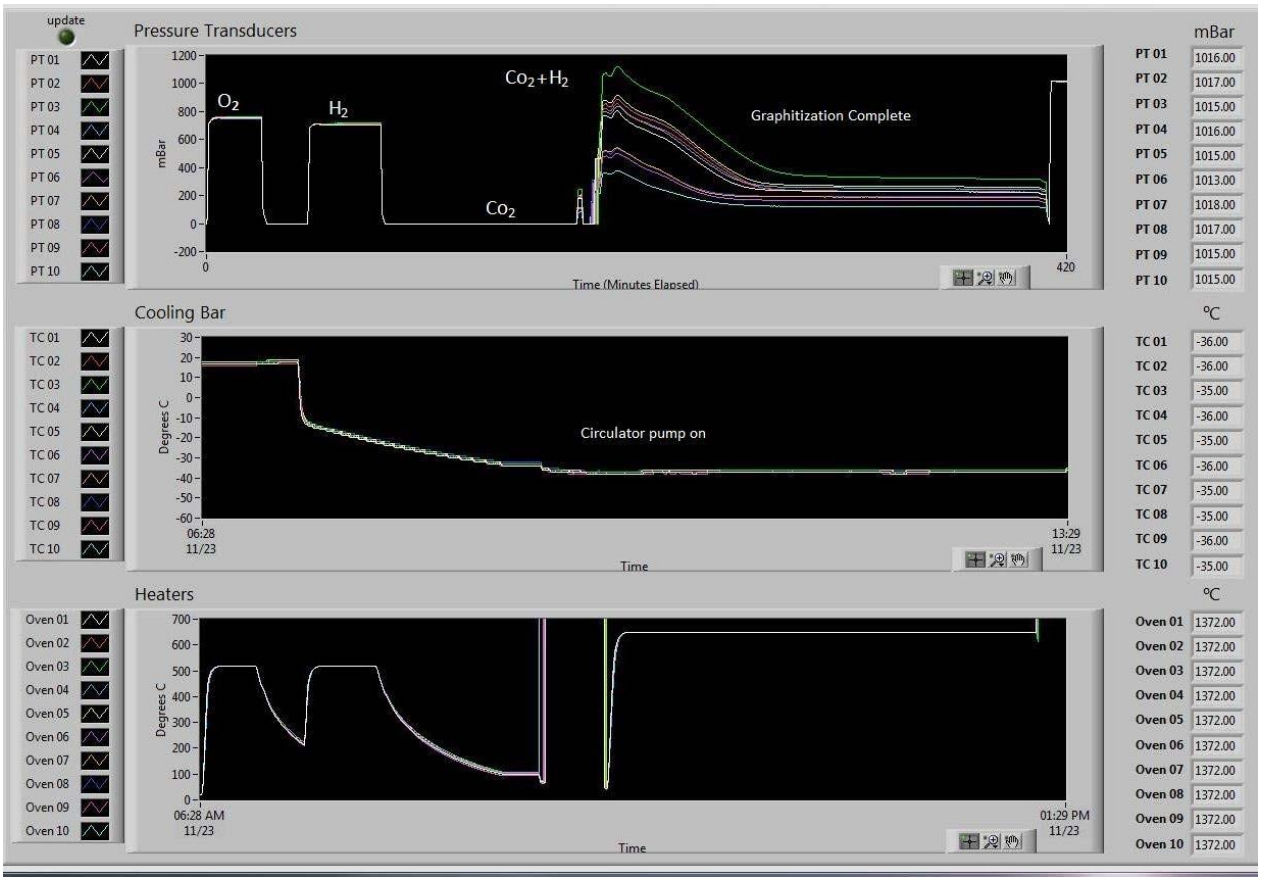

Figure 7: Monitoring records from for the graphitization line for the LAB and 1,2-Butanediol samples combusted in sealed quartz tubes. The main phases of graphitization are labeled on the plot of the pressure transducers (top), reading left to right: Fe oxidation (O_2); pumping; Fe reduction (H_2); pumping; sample release (CO_2); addition of H_2; graphitization. The middle plot shows the temperature of each cooling cup (water trap), and the bottom plot shows the temperature of each oven. Each plot shows the time in a different manner: start to finish in minutes (top); start time using 24-hr clock (middle); start time using AM/PM (bottom).

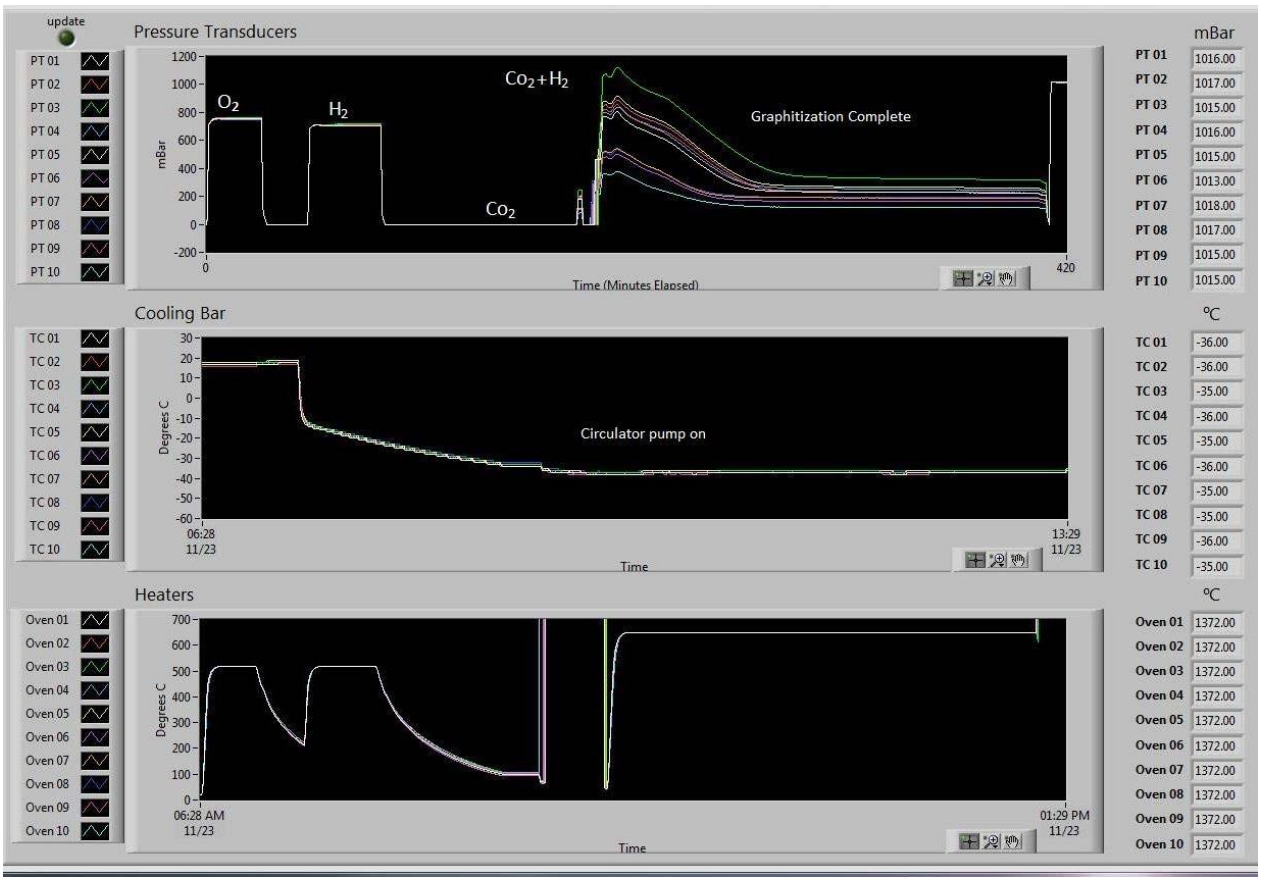

Figure 8: Monitoring records from the graphitization line for the LAB and 1,2-Butanediol samples combusted in the elemental analyzer. The main phases of graphitization are labeled on the plot of the pressure transducers (top), reading left to right: Fe oxidation (O_2); pumping; Fe reduction (H_2); pumping; sample release (CO_2); addition of H_2; graphitization. The middle plot shows the temperature of each cooling cup, and the bottom plot shows the temperature of each heater. Each plot shows the time in a different manner: st art to finish in minutes (top); start time using 24-hr clock (middle); start time using AM/PM (bottom)

3.3.2 Setup for AMS Analysis:

The ion source was thoroughly cleaned to remove any traces of previous higher level samples. Lead fluoride targets were then sputtered to provide further surface cleaning just before the measurements. The low level samples LAB and 1, 2-Butanediol were measured first in a group, and their results were calibrated against Ox-II standard measured in a subsequent group under the same conditions.

3.3.3 Result and discussion:

The results for all aliquots of both sample materials and both combustion methods are presented in table 2 (combustion yields), in table 3 (AMS raw data) and figures 9 to 12. Several of the aliquots were contaminated with ^{14}C in both the EA and Quartz Tube processes as can be seen in table 3 and figures 9 - 11. The reason for the lower yield of CO_2 from the quartz tube process was that despite cooling the sample to liquid nitrogen temperature at the base of the tube, the heat required to seal the quartz tube at the top, caused some of the sample to escape. All the of the results for LAB and 1,2- Butanediol presented in table 3 were calibrated using the Ox-II standard, which was measured in an AMS run immediately following the LAB and Butanediol measurements to avoid any ion source contamination from the much higher levels of ^{14}C in the Ox-II standard.

The results in table 3 are reported as a "Fraction of Modern Carbon" ($F^{14}C$), defined as

$$F^{14}C = A_{SN} / A_{ST},$$

where A_{SN} is the activity of the sample corrected for isotope fractionation in the sample formation and measurement process and A_{ST} is defined as the 95% of the activity of the Ox-I satandard [41]. The uncertainties quoted in table 3 and shown as error bars in figures 9 – 12 include the statistical uncertainties in the ^{14}C counts, and the ^{12}C and ^{13}C current measurements.

Table 2: Elemental Analyzer Combustion Quartz Tube Combustion Yield Comparison

Submitter ID	EA Combustion Yield	Quartz Tube Combustion Yield
LAB-1	87.4%	60.6%
LAB-2	88.4%	50.8%
LAB-4	84.0%	37.1%
LAB-4	87.9%	N/A *
LAB-5	88.9%	46.2%
1,2-B(SNO+)-1	46.7%	40.1%
1,2-B(SNO+)-2	48.5%	48.5%
1,2-B(SNO+)-3	53.9%	29.7%
1,2-B(SNO+)-4	48.8%	34.9%
1,2-B(SNO+)-5	53.9%	N/A *

* For these measurements, the balance did not provide a stable reading.

Table 3: Radiocarbon results – Raw data.

Lab ID	Submitter ID	Material	$F^{14}C$	±
Elemental Analyzer Combustion				
UOC-3147	Acetanilide EA-1	Acetanilide	0.21	0.06
UOC-3148	Acetanilide EA-2	Acetanilide	0.02	0.01
UOC-3127	LAB_EA-1	Linear Alkyl benzene	0.06	0.02
UOC-3128	LAB_EA-2	Linear Alkyl benzene	0.12	0.04
UOC-3129	LAB_EA-3	Linear Alkyl benzene	0.05	0.01
UOC-3130	LAB_EA-4	Linear Alkyl benzene	0.07	0.02
UOC-3131	LAB_EA-5	Linear Alkyl benzene	0.05	0.01
UOC-3137	1,2-B(SNO+)_EA-1	1,2,Butanediol	0.34	0.08
UOC-3138	1,2-B(SNO+)_EA-2	1,2,Butanediol	0.10	0.03
UOC-3139	1,2-B(SNO+)_EA-3	1,2,Butanediol	0.16	0.03
UOC-3140	1,2-B(SNO+)_EA-4	1,2,Butanediol	0.10	0.03
UOC-3141	1,2-B(SNO+)_EA-5	1,2,Butanediol	0.08	0.03
Sealed Quartz Tube Combustion				
UOC-3149	Acetanilide QTZ1	Acetanilide	0.04	0.02
UOC-3150	Acetanilide QTZ2	Acetanilide	0.02	0.01
UOC-3132	LAB_QTZ-1	Linear Alkyl benzene	0.99	0.75
UOC-3133	LAB_QTZ-2	Linear Alkyl benzene	0.08	0.03
UOC-3134	LAB_QTZ-3	Linear Alkyl benzene	0.08	0.03
UOC-3135	LAB_QTZ-4	Linear Alkyl benzene	0.07	0.02
UOC-3136	LAB_QTZ-5	Linear Alkyl benzene	0.09	0.03
UOC-3142	1,2-B(SNO+)_QTZ1	1,2,Butanediol	0.25	0.05
UOC-3143	1,2-B(SNO+)_QTZ2	1,2,Butanediol	0.21	0.06
UOC-3144	1,2-B(SNO+)_QTZ3	1,2,Butanediol	0.16	0.06
UOC-3145	1,2-B(SNO+)_QTZ4	1,2,Butanediol	0.06	0.02
UOC-3146	1,2-B(SNO+)_QTZ5	1,2,Butanediol	0.19	0.05

Linear Alkyl Benzene (LAB):

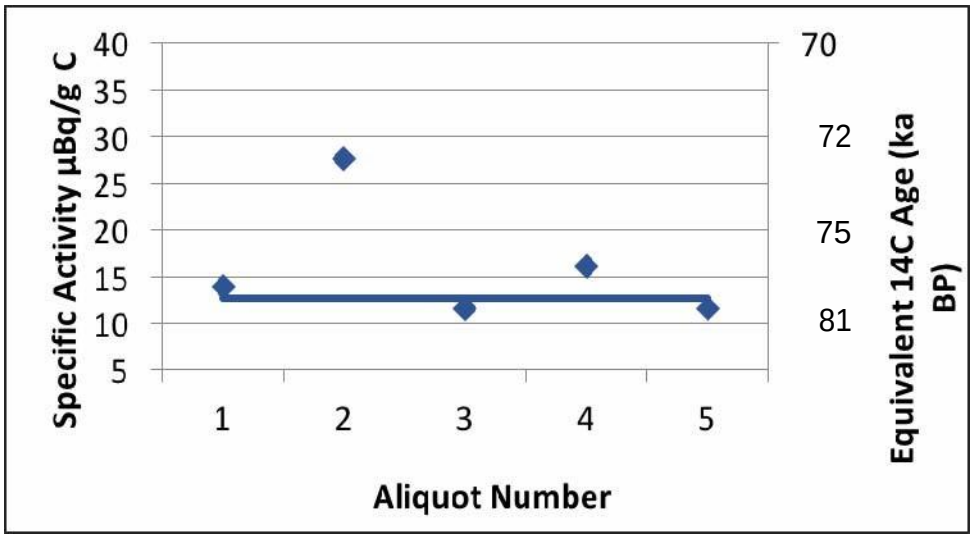

Figure 9: Results for individual aliquots of LAB combusted in an elemental analyzer. Activities were calculated using the $F^{14}C$ data in table 3 The straight line is the weighted mean of the 4 selected points = 12.7 ± 2.0 µBq/g.

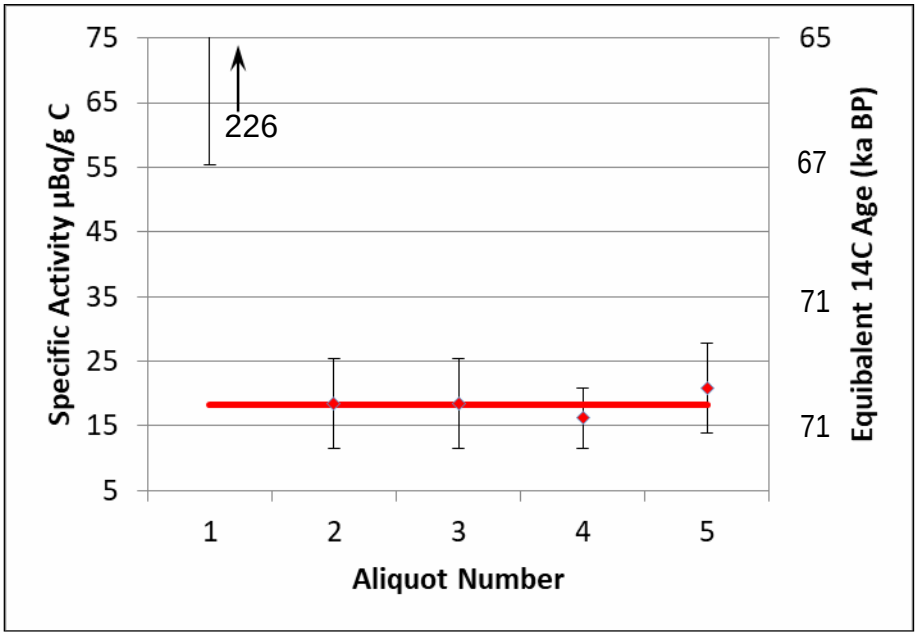

Figure 10: LAB combusted in sealed quartz tubes with activities calculated from the $F^{14}C$ in table 3. For these samples, some of the frozen material was lost due to the heat of the sealing process and so the yields were lower than expected and thus these data have larger errors. The straight line is the weighted mean of the 4 selected points: = 18.2 ± 2.0 µBq/g

Result for 1, 2 Butanediol:

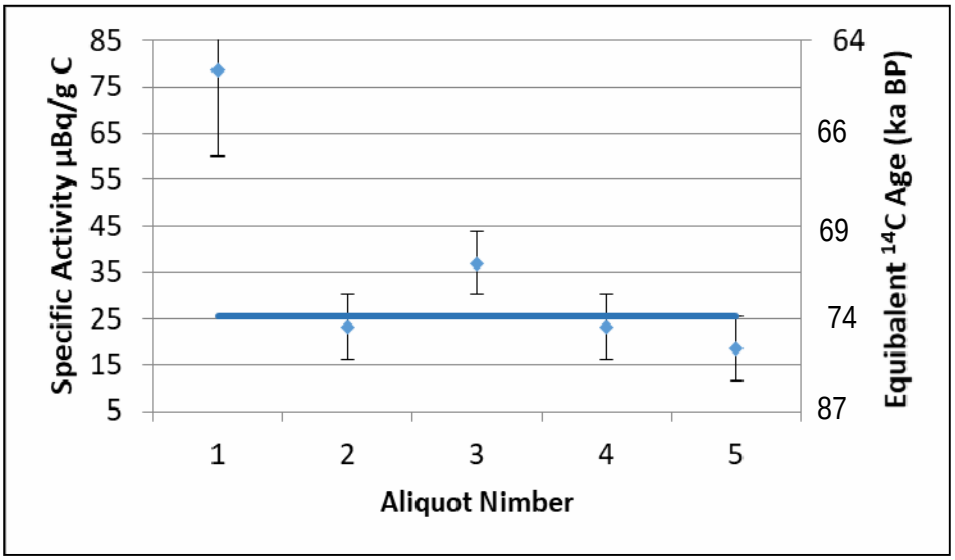

Figure 11: Butanediol combusted in elemental analyzer, activities calculated from the $F^{14}C$ in table 3. Tbe straight line is the weighted average of the 4 selected points = 25.4 ± 8.0 µBq/g

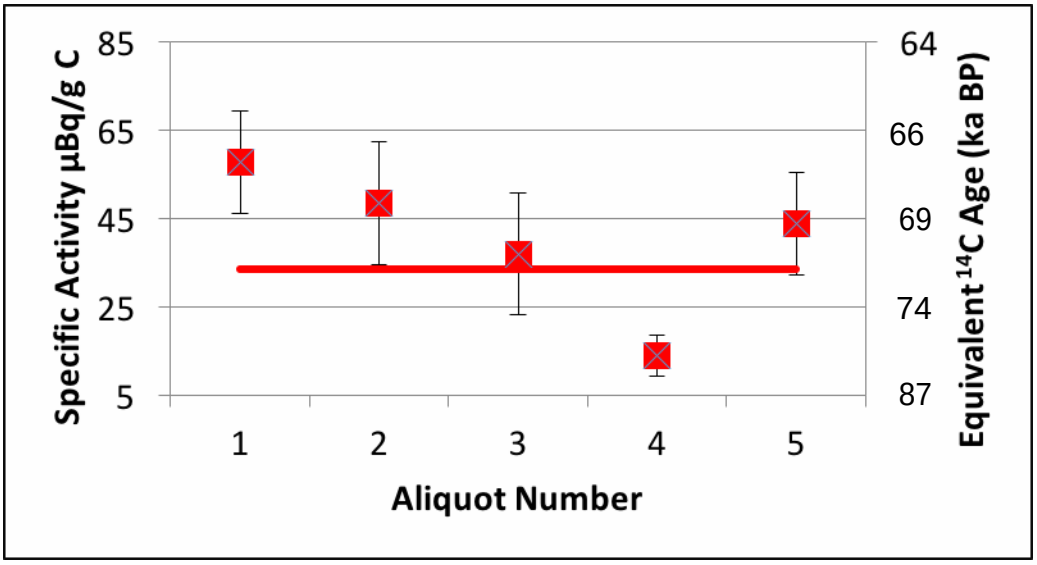

Figure 12: Butanediol combusted in sealed quartz tube, activities calculated from the $F^{14}C$ in table 3. The straight line is the weighted average of all 5 points = 33.6 ± 19.4 µBq/g

Summary:

The conclusion which can be drawn from these measurements, which was provided by the SNO+ physicists, is that although the ^{14}C concentration in the 1,2-Butanediol is approximately twice that of the LAB, it is sufficiently low to permit its use in the SNO+ NDBD; experiment However, before proceeding with the purchase of a large amount of the 1,2, Butanediol, it would be good to determine the level of ^{14}C contamination in several aliquots of the materials to be used used for SNO+.

This measurement was also an exploration of the detection limits of the Lalonde AMS combustion, graphitization and AMS systems. Such tests always require the analysis of blanks, with as little ^{14}C content as possible. As these measurements were far below the normal ^{14}C AMS measurement level, such blank material does not exist. However, the LAB, as it had been used in other large scintillation detectors, provided a very effective blank. From the LAB measurements, one can also conclude that all the cleaning steps are needed to reduce the ^{14}C contamination during the measurement. The quartz tube process, although normally cleaner, in the case of these liquid samples, is not the preferred method.

Chapter 4
Measurements of the nEXO materials

4.1 Materials for building the Time-projection chamber:

An important goal in the building of the n EXO detector is to enhance the sensitivity based on a proper selection of materials. One major source of reduction in this sensitivity in the radioactive decay of trace amounts of uranium and thorium isotopes naturally present tn the construction materials. In order to assess the quantity of these isotopes in the copper used to make the electrodes in the n EXO detector. AMS was used to analyze some samples of the copper. This study describes the analysis of the copper used to make the electrodes and see if there are any actinide elements whose radioactive decay would interfere with the measurements [42].

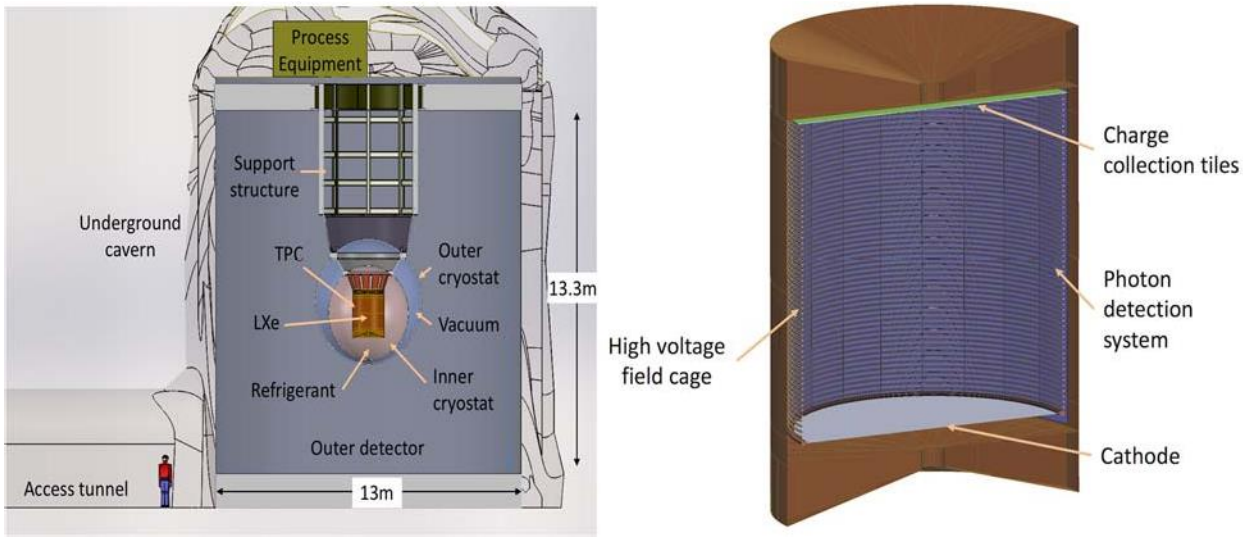

Figure 13: Cross- section views of the nEXO full system and time projection chamber detector [43].

4.2 The nEXO Liquid Xenon Detector:

The nEXO detector, like the EXO-200 detector is a time projection chamber (TPC). A Time projection chamber is a device used in particle physics to measure the energy and momentum of a charged particle. It is typically a cylindrical detector with an anode at one end and a high potential cathode at the other. For the nEXO detector, the anode is at ground potential and it supports an array of detector wires which determine the position of particle. The chamber is filled with liquid Xenon which produces electrons along the path of the charged particle. The axial electric field produced by the cathode and anodes guides the electrons along the electric field lines, perpendicular to the anode. Silicon photomultipliers, (SiPMs) detects scintillation light from particle interactions in the liquid Xe. The SiPMs are arranged behind the field-shaping rings on the circumference of the cylinder inside the TPC. The detectors on the anode give the electron signal as a function of time, so the trajectory's radial coordinates can be measured through its projection on the anode detectors. The time between when the particle ionizes the liquid and the electrons reaching the anode end is the drift time, which is used to calculate the axial position of the particle as a function of time.

The detector design is optimized to achieve a good energy resolution but this could be degraded be interference from radioactive elements. If the concentration of these elements is known, it can be used to calculate the number of the background events and their influence on the sensitivity of the detector. External (cosmic ray) interferences are eliminated by the location of the nEXO equipment 2 km underground in the Sudbury Neutrino observatory and by a containment system in which the TPC is located in a water tank to shield from the natural radioactivity in the walls of the cavern and which is equipped with photomultiplier tubes to track and reject any muon signals that reach the TPC.

4.2 Experimental

Thorium and uranium can be found at low concentrations in copper, which is one of the materials used for the electrodes in the nEXO experiment. Attempts to detect these elements at very low concentrations have proven difficult until the use of accelerator mass spectrometry (AMS). The measurements were all performed at the Lalonde AMS Laboratory using a 3 MV tandem accelerator mass spectrometer.

The use of AMS is effective way of determining the concentration of the actinides for a number of other applications, such as environmental analysis, nuclear forensics [46].

Even for the AMS method, the analysis of pure copper is a complicated measurement because no reference standards are available. It has only been demonstrated once [47]. Samples of the copper to be investigated (Aurubis copper) were made into target pieces (Figure 14). For comparison, copper target pieces that are used for other AMS analyses were also measured. Because it is difficult to make negative atomic ions from Uranium or Thorium, AMS often uses a molecule containing these metals to make the negative ions. The only elements available in the target to produce such molecules are copper, and possible traces of U and Th and cesium from the sputtering beam, after the initial few seconds of sputtering.

In order to determine the best molecules to use, tests were made using the low energy mass spectrometer of the AMS system. With the copper target mounted in the ion source, the injector magnet was scanned over its full mass range and the resulting ion currents were recorded in the Faraday cup before the accelerator entrance. The samples were loaded onto stainless target holders (figure 14 right) for the measurements.

Figure 14: (left image) Target, (right image), mounted on the target base (below) and loaded in the ion source "wheel" (top).

Molecules containing only copper are expected to be more abundant but those containing Th and U will be needed for the concentration measurement. Table 4 and Figure 15 show the currents of many molecular anions produced in the ion source using targets of only copper. A beam of $^{63}Cu_4{}^{65}Cu^-$ provided the highest current in usable mass range and so was used for normalization.

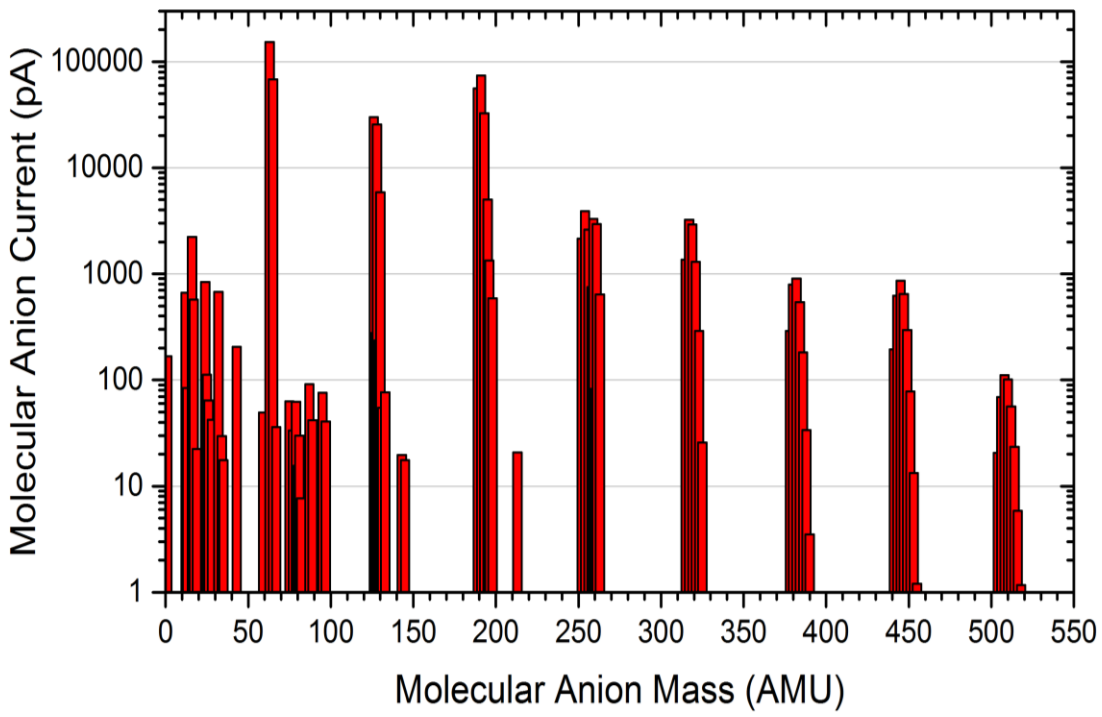

Figure 15: a mass spectrum taken using the ion source and scanning the injection magnet.

Table 4: Mass spectrum of copper clusters (from Cu-pin-in-Cu-target)

Magnetic field (T)	Normalized current (PA)	Mass (AMU)	Probable ions
0.642390	82.24	260	$^{65}Cu_4^-$
0.643700	2955.67	261	$^{63}Cu^{\bullet}{}^{65}Cu^{\bullet}{}^{133}Cs^-$
0.646140	639.34	263	$^{65}Cu_2{}'{}^{133}Cs^-$
0.707320	1360.00	315	$^{63}Cu_5^-$
0.709570	**3245.19**	**317**	$\mathbf{^{63}Cu_4{}'{}^{65}Cu^-}$
0.711850	2929.37	319	$^{63}Cu_3{}'{}^{65}Cu_2^-$
0.714050	1294.21	321	$^{63}Cu_2{}'{}^{65}Cu_3^-$
0.716240	289.86	323	$^{63}Cu^{65}Cu_4^-$
0.718580	25.81	325	$^{65}Cu_5^-$

Table 5: Mass spectruem of copper clusters with ^{238}U. Count-rates were also normalized to 500 nA total outputs, in unit of counts per 600 seconds (or c/10m). The actual counting time spent on each beam varied from 100 to 1000 seconds.

^{238}U beams	Counts per 600 seconds
$^{238}U^{-} \rightarrow {}^{238}U^{+3}$	2
$^{238}U^{16}O^{-} \rightarrow {}^{238}U^{+3}$	1210
$^{238}U^{63}Cu^{-} \rightarrow {}^{238}U^{+3}$	56
$^{238}U^{63}Cu_2^{-} \rightarrow {}^{238}U^{+3}$	61
$^{238}U^{63}Cu_3^{-} \rightarrow {}^{238}U^{+3}$	48
$^{238}U^{63}Cu_4^{-} \rightarrow {}^{238}U^{+3}$	108
$^{238}U^{133}Cs^{-} \rightarrow {}^{238}U^{+3}$	8
$^{238}U^{63}Cu^{133}Cs^{-} \rightarrow {}^{238}U^{+3}$	33

Table 5 shows the molecular anions from a target which contains ^{238}U as well as copper. In this measurement, no molecules containing Th were found in the cupper target. The largest number of molecules produced in this test were the ones containing oxygen, but the oxygen content will be very much dependent on the the residual oxygen in the vacuum system or in the target material. As this could vary during the analysis and so would not necessarily produce a representative beam from each target, UO- was not considered suitable for trace U/Th detection in copper. So the procedure to detect traces U/Th in copper used $^{238}U^{63}Cu_4^{-}$ and $^{232}Th^{63}Cu_4^{-}$ cluster ions. Because no ^{232}Th was seen in the standard copper target, it was assumed to have the same molecular form as the ^{238}U. To analyze the U and Th anions with the injector magnet, the ion source voltage had to be reduced from 35 kV to 25 kV.

4.3 Set up of the AMS system

The experiment involved three stages. First, for AMS system tuning, gold oxide was mixed with silver powder and packed in a Cu AMS target holders, back pressed by a copper pin. Secondly, two samples of the nEXO Aurubis^{TM} copper were machined into solid target pieces (figure 13a) and thirdly, two standard AMS copper target filed with copper pin were analyzed for comparison.

The following experiment steps were used:

- the entire AMS system was first well tuned on a very stable gold pilot beam
  - $^{197}Au^{-} \rightarrow {}^{197}Au^{+3}$
- the change in the tuning for the parent $^{238}U^{63}Cu_4^-$ and $^{232}Th^{63}Cu_4^-$ molecular ions was calculated for the magnets and electric analyzers, stterers and lenses using equations 2.3 and 2.4.
- For the trace elements, ion masses up to 490 AMU ($^{238}U^{63}Cu_4^-$) had to be analyzed by the injection magnet, so the SO-110B source was operated with 7 kV target voltage and 18 k to produce 25 kev negative ions for injecting the molecular anions of U and Th.
- For the first measurements, the cesium sputter current was controlled by setting the cesium reservoir temperature to 95 °C
- AMS measurement of trace U and Th in the copper target used the automated slow sequential injection procedure for both ^{238}U and ^{232}Th set for 20 seconds per step.
  - $^{238}U^{63}Cu_4^- \rightarrow {}^{238}U^{+3}$,
  - $^{232}Th^{63}Cu_4^- \rightarrow {}^{238}U^{+3}$,
  - $^{63}Cu_4{}^{65}Cu^- \rightarrow {}^{63}Cu^{+1}$

4.4 The Results

The tables 6 and 7 show the number the particles counted, normalized to a counting time of 5000 seconds. The limited concentration of ^{232}Th and ^{238}U in the copper samples is indicated by small number of counts. In the first table the number of U in the Aurubis copper is the same for both targets and more than twice the number from AMS standard copper. Since this was the first measurement of these samples, it was suspected that the surface of the Aurubis copper might have been contaminated during the machining process. After Cs sputter cleaning of the surfaces of all targets for an hour, a second measurement was started using a lower ion source caesium current (Cs reservoir temperature 25°C). Theses measurements, shown in table 9, again indicated that there was more Uranium in the Aurubis copper than in the AMS copper.

Table 6: Moderate Ion Source Current – Caesium reservoir at 95ºC Particles counted per 5000 seconds.

Sample Number	**$^{63}Cu^{+1}$ (HE Offset Faraday Cup)**	**$^{238}U^{+3}$ (Gas Ionization Detector)**	**$^{232}Th^{+3}$ (Gas Ionization Detector)**
AMS Cu A1	4.25E+13	39	49
AMS Cu A3	3.48E+13	40	23
Aurub is Cu A1	4.44E+13	85	1
Aurub is Cu A3	4.75E+13	85	3

Table7: After Cs sputter cleaning of surfaces of all targets for an hour, with low ion Source Current - Caesium reservoir at 25ºC Particles counted per 5000 seconds.

Sample Number	**$^{63}Cu^{+1}$ (HE Offset Faraday Cup)**	**$^{238}U^{+3}$ (Gas Ionization Detector)**	**$^{232}Th^{+3}$ (Gas Ionization Detector)**
AMS Cu A1	1.85E+12	7	1
AMS Cu A3	1.47E+12	3	2
Aurubis Cu A1	1.76E+12	48	2
Aurubis Cu A3	1.59E+12	45	4

Summary

In both sets of measurements, the Aurubis copper was found to be more contaminated that the copper used for making the AMS targets. This led the builders of the nEXO TPC to look into using this source of copper rather than Aurubis.

To calculate the effect of the U and Th on the detector, an absolute measurement of their concentration (number of U or Th atoms per g of copper) is needed. AMS measurements are usually made relative to a standard reference material, but none exists for U or Th in copper. However, a basic knowledge of the efficiencies of the ion transmission through the AMS system can be used to obtain an estimate of the concentration

The success of this measurement can be attributed to the fact that AMS is able to detect low count rates from the almost pure samples. So the AMS measurement provided comparison of the trace U concentration in the AMS copper was much lower than the Aurubis copper. UO^- still cannot be considered suitable for trace U/Th detection in copper. It was identified that the

use of the $^{63}Cu_4{\cdot}^{65}Cu^-$ cluster should provide more accurate normalizes to the formation of $U{\cdot}^{63}Cu_4^-$ and $Th{\cdot}^{63}Cu_4^-$ clusters because it is similar molecular composition

Chapter 5

Conclusion

The goal of this work was twofold as it reflects the two main sections of this work:

In the first part of this thesis, measuring the trace level of ^{14}C in the materials for use in the SNO+ was also a step towards the goal of determining the interference levels. Accelerator mass spectrometry effectively accelerates ions to achieve exceptionally high kinetic energies prior to performing mass diagnostics on the given sample. This analytics procedure was effective in the separation of uncommon isotopes from abundant adjacent isotopes. Results show the measurements of the ^{14}C concentration in the 1,2-Butanediol were as sufficiently low compared to the Linear Alkyl benzene. In order to ensure consistent data, every step of decontamination was necessary in order to reduce ion source contamination. Each stage was successful. The Quartz Tube process, although normally sterile, in the case of these liquid samples is not the preferred method.

In the second part of this thesis, when measuring trace amounts of U and Th in copper, the detection limit is controlled by tuning AMS system. Gold oxide with silver in was packed into a Cu AMS target holder. The AMS measurement provided an estimate of the trace U and Th concentrations in the copper and showed that the AMS copper was probably less contaminated than the Aurubis copper.

Although promising, in order to determine the actual concentration of the U and Th in the copper, a reference standard will be required. This method could be used to successfully detach atomic isobars. Although the process is clear, further research and development is needed.

Bibliography

[1] Morrissey, D. J., Seaborg, G. T., & Loveland, W. D. (2006). *Modern Nuclear Chemistry*. Wiley-Interscience. ISBN 0-471-11532-0.

[2] Magill, J., & Galy, J. (2004). *Radioactivity radionuclides radiation* (Vol. 1). Springer Science & Business Media.

[3] Close, F. (2012). *Neutrino*. Oxford University Press.

[4] Brown, L. M. (1978). The idea of the neutrino. *Physics Today*, *31*(9), 23-28.

[5] Carrol, S. (2009). *Ada Lovelace Day: Chien-Shiung Wu*. Retrieved from Discover Magazine: http://blogs.discovermagazine.com/cosmicvariance/2009/03/25/ada-lovelace-day-chien-shiung-wu/#.W3mEmvWerIV

[6] Banerjee, A., Bridges, C. A., Yan, J. Q., Aczel, A. A., Li, L., Stone, M. B., ... & Bhattacharjee, S. (2016). Proximate Kitaev quantum spin liquid behaviour in a honeycomb magnet. *Nature materials*, *15*(7), 733-740. doi:10.1038/nmat4604

[7] Elliott, S. R., Hahn, A. A., & Moe, M. K. (1987). Direct evidence for two-neutrino double-beta decay in Se 82. *Physical Review Letters*, *59*(18), 2020-2023. doi:10.1103/PhysRevLett.59.2020.

[8] Fireman, E. (1948, January). Double Beta-Decay. In *Physical Review* (Vol. 74, No. 9, pp. 1238-1238). doi:10.1103/PhysRev.74.1201.

[9] Furry, W. H. (1939). On transition probabilities in double beta-disintegration. *Physical Review*, *56*(12), 1184-1193. doi:10.1103/PhysRev.56.1184.

[10] Gando, A., Gando, Y., Hachiya, T., Hayashi, A., Hayashida, S., Ikeda, H., ... & Matsuda, S. (2016). Search for Majorana neutrinos near the inverted mass hierarchy region with KamLAND-Zen. *Physical review letters*, *117*(8), 082503. doi: https://doi.org/10.1103/PhysRevLett.117.082503.

[11] Giuliani, A., & Poves, A. (2012). Neutrinoless double-beta decay. *Advances in High Energy Physics*, *2012*. 857016. doi:10.1155/2012/857016.

[12] Sergeenkov, Y. V. (1989). Nuclear data sheets for A= 130. *Nuclear Data Sheets*, *58*(4), 765-870.

[13] Avignone III, F. T., Elliott, S. R., & Engel, J. (2008). Double beta decay, Majorana neutrinos, and neutrino mass. *Reviews of Modern Physics*, *80*(2), 481.

[14] Ho, C. M., & Scherrer, R. J. (2013). Anapole dark matter. *Physics Letters B*, *722*(4-5), 341-346. https://doi.org/10.1016/j.physletb.2013.04.039.

[15] Majorana, E. (1981). A symmetric theory of electrons and positrons. *Soryushiron Kenkyu Electronics*, *63*(3), 149-162. doi:10.1007/978-3-540-48095-2_10.

[16] Nadj-Perge, S., Drozdov, I. K., Li, J., Chen, H., Jeon, S., Seo, J., ... & Yazdani, A. (2014). Observation of Majorana fermions in ferromagnetic atomic chains on a superconductor. *Science*, 1259327. *346*(6209), 602-607. doi: 10.1126/science.1259327.

[17] Patrignani, C., & Particle Data Group. (2016). Review of particle physics. *Chinese physics C*, *40*(10), 100001. doi:10.1088/1674-1137/40/10/100001.

[18] Beringer, J., Arguin, J. F., Barnett, R. M., Copic, K., Dahl, O., Groom, D. E., ... & Yao, W. M. (2012). Review of particle physics. *Physical Review D-Particles, Fields, Gravitation and Cosmology*, *86*(1), 292.

[19] Aharmim, B., Cleveland, B. T., Dai, X., Doucas, G., Farine, J., Fergani, H., ... & Lange, R. (2009). High sensitivity measurement of 224Ra and 226Ra in water with an improved hydrous titanium oxide technique at the Sudbury Neutrino Observatory. *Nuclear Instruments and Methods in Physics Research Section A: Accelerators, Spectrometers, Detectors and Associated Equipment*, *604*(3), 531-535. doi: http://dx.doi.org/10.1016/j.nima.2009.01.227.

[20] Bellini, G., Benziger, J., Bick, D., Bonfini, G., Bravo, D., Caccianiga, B., ... & Chavarria, A. (2014). Neutrinos from the primary proton–proton fusion process in the Sun. *Nature*, *512*(7515), 383. doi:10.1038/nature13702.

[21] Castelvecchi, D. (2015). *Neutrinos found to switch to elusive 'tau' flavour. Nature.* Retrieved from http://www.nature.com/news/neutrinos-found-to-switch-to-elusive-tau-flavour-1.17777.

[22] Mertens, S. (2016, May). Direct Neutrino Mass Experiments. In *Journal of Physics: Conference Series* (Vol. 718, No. 2, p. 022013). IOP Publishing. doi: https://doi.org/10.1088/1742-6596/718/2/022013.

[23] Maneira, J., & Sno+ Collaboration. (2013). The SNO+ experiment: status and overview. In *Journal of Physics: Conference Series* (Vol. 447, No. 1, p. 012065). IOP Publishing.

[24] Carlton University. (2017). *EXO - Enriched Xenon Observatory*. Retrieved March 29, 2017 from http://www.physics.carleton.ca/exo.

[25] Farine, J. (2006). EXO - *The Enriched Xenon Observatory for the search of neutrinoless double beta decay of 136Xe. Queen's University*. Retrieved March 29, 2017 from http://www.queensu.ca/physics/exo-enriched-xenon-observatory-search-neutrinoless-double-beta-decay-136xe.

[26] EXO-200. (2016). *EXO: About the experiment*. Retrieved March 29, 2017 from https://www-project.slac.stanford.edu/exo/about.html

[27] St-Jean, G., Kieser, W. E., Crann, C. A., & Murseli, S. (2017). Semi-Automated Equipment for CO 2 Purification and Graphitization at the AE Lalonde AMS Laboratory (Ottawa, Canada). *Radiocarbon*, *59*(3), 941-956.

[28] Litherland, A. E., Paul, M., Allen, K. W., & Gove, H. E. *Philosophical Transactions of the Royal Society of London A: Mathematical, Physical and Engineering Sciences*. *A*, *323*(1569), 5-21.

[29] Kieser, W. E., Zhao, X. L., Clark, I. D., Cornett, R. J., Litherland, A. E., Klein, M., Mous, D. J. W, & Alary, J. F. (2015). The André E. Lalonde AMS Laboratory–the new accelerator mass spectrometry facility at the University of Ottawa. *Nuclear Instruments and Methods in Physics Research Section B: Beam Interactions with Materials and Atoms*, *361*, 110-114. doi: https://doi.org/10.1016/j.nimb.2015.03.014

[30] Bronk, C. R., & Hedges, R. E. M. (1989). Use of the CO 2 source in radiocarbon dating by AMS. *Radiocarbon*, *31*(3), 298-304. doi:10.1017/s0033822200011838.

[31] Zhao, X. L., Eliades, J., Litherland, A. E., Kieser, W. E., Cornett, J., & Charles, C. R. J. (2013). On□line HfF5−/WF5− separation in an O2□filled radiofrequency quadrupole gas cell. *Rapid Communications in Mass Spectrometry*, *27*(24), 2818-2822.

[32] Siri, W. (1947). A mass spectroscope for analysis in the low mass range. *Review of Scientific Instruments*, *18*(8), 540-545.

[33] Hellborg, R., & Skog, G. (2008). Accelerator mass spectrometry. *Mass Spectrometry Reviews*, *27*(5), 398-427. doi: 10.1002/mas.20172.

[34] Klein, M., Gottdang, A., & Mous, D. J. W. (2013). High-Current 14 C Measurements on an HVE 1MV AMS System. *Radiocarbon*, *55*(2), 224-230. doi:10.2458/azu_js_rc.55.16052.

[35] Ramsey, C. B., Ditchfield, P., & Humm, M. (2004). Using a gas ion source for radiocarbon AMS and GC-AMS. *Radiocarbon*, *46*(1), 25-32. doi:10.1017/S003382220003931X.

[36] Yun-Chong, F., Wei-Jian, Z., Hua, D., Peng, C., Xiao-Lei, Z., Qi, L., ... & Wen-Nian, Z. (2015). A preliminary study of small-mass radiocarbon sample measurement at Xi'an-AMS. *Chinese Physics C*, *39*(3), 036202.

[37] SNO+. (2018). *Home Page*. Retrieved From SNO+: http://snoplus.phy.queensu.ca/Home.html.

[38] O'Keeffe, H. M., O'sullivan, E., & Chen, M. C. (2011). Scintillation decay time and pulse shape discrimination in oxygenated and deoxygenated solutions of linear alkylbenzene for the SNO+ experiment. *Nuclear Instruments and Methods in Physics Research Section A: Accelerators, Spectrometers, Detectors and Associated Equipment*, *640*(1), 119-122.

[39] Biller, S., Manecki, S., & SNO+ collaboration. (2017, September). A New Technique to Load 130Te in Liquid Scintillator for Neutrinoless Double Beta Decay Experiments. In *Journal of Physics: Conference Series* (Vol. 888, No. 1, p. 012084). IOP Publishing. Series 10.1088/1742-6596/888/1/012084.

[40] Litherland, A. E., Zhao, X.□L., et KIESER, W. E. Mass spectrometry with accelerators. *Mass spectrometry reviews*, 2011, vol. 30, no 6, p. 1037-1072. Doi: **https://doi.org/10.1002/mas.20311**.

[41] Erikson Senström, K., Skog, Gl, Georgiadu, E., Genberg, J., Johansson, A., A guide to radiocarbon units and calculations, Internal Report LUNFD6(NFFR-3111)/1-17/(2011), Lund University, Department of Physics (2011).

https://www.hic.ch.ntu.edu.tw/AMS/A%20guide%20to%20radiocarbon%20units%20and%20calculations.pdf

[42] LCTPC. (2013). *Working Principle of a Time Projection Chamber Homepage*. Retrieved From LCTPC: https://www.lctpc.org/e8/e57671/

[43] Albert, J. B., Anton, G., Arnquist, I. J., Badhrees, I., Barbeau, P., Beck, D., ... & Brunner, T. (2017). Sensitivity and Discovery Potential of nEXO to Neutrinoless Double Beta Decay. *arXiv preprint arXiv:1710.05075*.

[44] Dolinski, M. J., & EXO Collaboration. (2012). The Enriched Xenon Observatory: EXO-200 and Ba+ tagging. *Nuclear Physics B-Proceedings Supplements*, *229*, 124-127.

[45] Licciardi, C., & nEXO Collaboration. (2017, September). The sensitivity of the nEXO experiment to Majorana neutrinos. In *Journal of Physics: Conference Series* (Vol. 888, No. 1, p. 012237). IOP Publishing.

[46] Cornett, R. J., Kazi, Z. H., Zhao, X. L., Chartrand, M. G., Charles, R. J., & Kieser, W. E. (2015). Actinide measurements by AMS using fluoride matrices. *Nuclear Instruments and Methods in Physics Research Section B: Beam Interactions with Materials and Atoms*, *361*, 317-321.

[47] Famulok, N., Faestermann, T., Fimiani, L., Gómez-Guzmán, J. M., Hain, K., Korschinek, G., ... & Schönert, S. (2015). Ultrasensitive detection method for primordial nuclides in copper with Accelerator Mass Spectrometry. *Nuclear Instruments and Methods in Physics Research Section B: Beam Interactions with Materials and Atoms*, *361*, 193-196.